Intermodel Uncertainty in ENSO Amplitude Change Tied to Pacific Ocean Warming Pattern

XIAO-TONG ZHENG

Physical Oceanography Laboratory/CIMST, Ocean University of China and Qingdao National Laboratory for Marine Science and Technology, and Key Laboratory of Ocean–Atmosphere Interaction and Climate in Universities of Shandong, Ocean University of China, Qingdao, China

SHANG-PING XIE

Scripps Institution of Oceanography, University of California San Diego, La Jolla, California, and Physical Oceanography Laboratory/CIMST, Ocean University of China and Qingdao National Laboratory for Marine Science and Technology, Qingdao, China

LIANG-HONG LV

Physical Oceanography Laboratory/CIMST, Ocean University of China and Qingdao National Laboratory for Marine Science and Technology, and Key Laboratory of Ocean–Atmosphere Interaction and Climate in Universities of Shandong, Ocean University of China, Qingdao, China

ZHEN-QIANG ZHOU

Physical Oceanography Laboratory/CIMST, Ocean University of China and Qingdao National Laboratory for Marine Science and Technology, Qingdao, China

(Manuscript received 31 December 2015, in final form 6 July 2016)

ABSTRACT

How El Niño–Southern Oscillation (ENSO) will change under global warming affects changes in extreme events around the world. The change of ENSO amplitude is investigated based on the historical simulations and representative concentration pathway (RCP) 8.5 experiments in phase 5 of the Coupled Model Intercomparison Project (CMIP5). The projected change in ENSO amplitude is highly uncertain with large intermodel uncertainty. By using the relative sea surface temperature (SST) as a measure of convective instability, this study finds that the spatial pattern of tropical Pacific surface warming is the major source of intermodel uncertainty in ENSO amplitude change. In models with an enhanced mean warming in the eastern equatorial Pacific, the barrier to deep convection is reduced, and the intensified rainfall anomalies of ENSO amplify the wind response and hence SST variability. In models with a reduced eastern Pacific warming, conversely, ENSO amplitude decreases. Corroborating the mean SST pattern effect, intermodel uncertainty in changes of ENSO-induced rainfall variability decreases substantially in atmospheric simulations forced by a common ocean warming pattern. Thus, reducing the uncertainty in the Pacific surface warming pattern helps improve the reliability of ENSO projections. To the extent that correcting model biases favors an El Niño–like mean warming pattern, this study suggests an increase in ENSO-related SST variance likely under global warming.

1. Introduction

El Niño–Southern Oscillation (ENSO) is the dominant mode of tropical Pacific climate variability, with global impact on climate and society (McPhaden et al. 2006). Equatorial Pacific sea surface temperature (SST) anomalies are widely used to measure ENSO intensity. El Niño events are characterized by positive SST anomalies in the eastern equatorial Pacific and weak negative SST anomalies in the western equatorial Pacific (Philander 1990). This anomalous SST gradient shifts atmospheric convection eastward, leading to westerly wind anomalies along the equator. The westerly wind anomalies in turn suppress the upwelling in the eastern equatorial Pacific that maintains the east–west SST

Corresponding author address: Xiao-Tong Zheng, College of Oceanic and Atmospheric Sciences, Ocean University of China, Qingdao 266100, China.
E-mail: zhengxt@ouc.edu.cn

DOI: 10.1175/JCLI-D-16-0039.1

gradient. This Bjerknes (1969) positive feedback amplifies El Niño events. The ENSO-induced anomalous convection is the essential atmospheric component of Bjerknes feedback (hereafter convective feedback), driving atmospheric circulation and influencing global climate via teleconnections (Horel and Wallace 1981). ENSO is the important source of predictability on seasonal to interannual time scales.

As the leading ocean–atmosphere coupled mode in the tropics, how ENSO changes in the future is important for regional projections of interannual variability and extreme events. Climate models disagree on how SST amplitude of ENSO will change under increasing greenhouse forcing (Collins et al. 2010; Stevenson 2012; Cai et al. 2015a), limiting the reliability of regional climate projections (Xie et al. 2015). More recently, several robust projected changes in characteristics of ENSO emerged: Even though the SST amplitude does not show a robust response to global warming, the El Niño–induced rainfall variability increases in the central and eastern equatorial Pacific (Power et al. 2013). This change in ENSO rainfall leads to more extreme El Niño events in future climate projections (Cai et al. 2014) and an eastward shift and intensification of ENSO teleconnections over the Pacific and North America (Zhou et al. 2014).

Why does the ENSO rainfall variability increase and shift eastward despite a lack of consistent response in ENSO SST to global warming? Recent studies have suggested that the spatial pattern of SST warming plays an important role (Power et al. 2013; Cai et al. 2014; Chung et al. 2014; Zhou et al. 2014). Changes in tropical convection are strongly influenced by the ocean surface warming pattern (Xie et al. 2010; Chadwick et al. 2013; Huang et al. 2013). In most future projections, the SST increase peaks on the equator in the tropical Pacific (in the meridional direction) due to reduced evaporative damping and amplifies toward the eastern Pacific (in the zonal direction) with a weakened Walker circulation (Liu et al. 2005; Vecchi and Soden 2007a). This El Niño–like ocean warming pattern induces more precipitation in the mean over the equatorial Pacific following the ''warmer get wetter'' mechanism (Xie et al. 2010). In the multimodel ensemble mean, the enhanced warming in the eastern equatorial Pacific leads to increased rainfall variability associated with ENSO (Power et al. 2013; Cai et al. 2014). This intensified rainfall response to ENSO is robust despite large disagreement among models with regard to changes in the SST amplitude of ENSO. While the amplified rainfall response represents a robust change in ENSO dynamics under global warming, the large spread among models in ENSO amplitude change remains of great concern.

There are large uncertainties among different datasets concerning the spatial SST warming pattern in the tropical Pacific (Vecchi et al. 2008; Deser et al. 2010). Several studies suggest that the pattern is El Niño–like with more warming in the eastern equatorial Pacific and a weakened Walker circulation (Tokinaga et al. 2012), while other studies indicate that the warming pattern is La Niña–like with an enhanced Walker circulation during the last 100 years (Cane et al. 1997; L'Heureux et al. 2013). The ocean warming pattern also varies among models, and the intermodel spread is the main source of uncertainty in future projections of rainfall and atmospheric circulation changes (Ma and Xie 2013; Long et al. 2016). Understanding the role of the mean warming pattern in the intermodel spread in ENSO amplitude change is of importance.

The present study investigates the changes in ENSO amplitude under global warming based on the multimodel ensemble from phase 5 of the Coupled Model Intercomparison Project (CMIP5). Here we show that the mean SST warming pattern controls the ENSO amplitude response to global warming including the large intermodel spread. An enhanced warming in the eastern equatorial Pacific reduces the barrier of mean SST to the tropical convection threshold, enhancing convective feedback onto El Niño and increasing ENSO amplitude in SST. Additional atmospheric general circulation model (AGCM) experiments show that ENSO-induced rainfall variability increases much more in a spatially patterned warming experiment than in the uniform warming experiment, corroborating the importance of mean state changes for ENSO.

The rest of the paper is organized as follows. Section 2 briefly describes the model datasets and methods used in this study. Section 3 examines the response of ENSO amplitude to global warming and the relationship with ocean mean warming pattern in CMIP5 models. Section 4 examines the convective feedback change in AGCMs. Section 5 is a summary with discussion.

2. Datasets and methods

We use the output of 22 models from the World Climate Research Programme CMIP5 multimodel ensemble organized by the Program for Climate Model Diagnosis and Intercomparison for the Intergovernmental Panel on Climate Change Fifth Assessment Report (Table 1). Two sets of simulations are analyzed to examine the response of ENSO variability to global warming (Taylor et al. 2012): We compare the historical climate experiments (historical run) with the representative concentration pathway 8.5 (RCP8.5) experiments to investigate how the ENSO changes under global

TABLE 1. The 22 CMIP5 models used in this study. (Expansions of acronyms are available online at http://www.ametsoc.org/PubsAcronymList.)

Model name	Institute (country)	Length of PI-control run (yr)
BCC_CSM1.1	Beijing Climate Center, China Meteorological Administration (China)	500
CanESM2	Canadian Centre for Climate Modelling and Analysis (Canada)	996
CCSM4	National Center for Atmospheric Research (United States)	501
CNRM-CM5	Centre National de Recherches Météorologiques (France)	850
CSIRO Mk3.6.0	Commonwealth Scientific and Industrial Research Organisation in collaboration with the Queensland Climate Change Centre of Excellence (Australia)	500
FGOALS-g2	State Key Laboratory of Numerical Modeling for Atmospheric Sciences and Geophysical Fluid Dynamics (China)	700
FGOALS-s2	State Key Laboratory of Numerical Modeling for Atmospheric Sciences and Geophysical Fluid Dynamics (China)	501
GFDL CM3	NOAA/Geophysical Fluid Dynamics Laboratory (United States)	500
GFDL-ESM2G	NOAA/Geophysical Fluid Dynamics Laboratory (United States)	500
GFDL-ESM2M	NOAA/Geophysical Fluid Dynamics Laboratory (United States)	500
HadGEM2-CC	Met Office Hadley Centre (United Kingdom)	240
HadGEM2-ES	Met Office Hadley Centre (United Kingdom)	576
INM-CM4.0	Institute of Numerical Mathematics (Russia)	500
IPSL-CM5A-LR	L'Institut Pierre-Simon Laplace (France)	1000
IPSL-CM5A-MR	L'Institut Pierre-Simon Laplace (France)	300
MIROC5	University of Tokyo, Atmosphere and Ocean Research Institute, National Institute for Environmental Studies, and Japan Agency for Marine-Earth Science and Technology (Japan)	700
MIROC-ESM	University of Tokyo, Japan Agency for Marine-Earth Science and Technology, Atmosphere and Ocean Research Institute, and National Institute for Environmental Studies (Japan)	531
MIROC-ESM-CHEM	University of Tokyo, Japan Agency for Marine-Earth Science and Technology, Atmosphere and Ocean Research Institute, and National Institute for Environmental Studies (Japan)	255
MPI-ESM-LR	Max Planck Institute for Meteorology (Germany)	1000
MPI-ESM-MR	Max Planck Institute for Meteorology (Germany)	1000
MRI-CGCM3	Meteorological Research Institute (Japan)	500
NorESM1-M	Norwegian Climate Centre (Norway)	501

warming. The historical experiments are forced by historical greenhouses gases, aerosols, and other radiative forcing, while the RCP8.5 experiments are subject to increasing radiative forcing that reaches about $+8.5\,W\,m^{-2}$ near 2100 (equivalent to >1370 ppm in CO_2 concentration). For each model only one member run (r1i1p1) is analyzed in this study because only one run is available for many models. We choose 90 years each in the twentieth (1911–2000) and twenty-first (2006–95) centuries to represent present-day and future climates, respectively. To test the significance of ENSO amplitude change in future projection, we also analyzed the preindustrial control run with constant radiative forcing in each model (see Table 1). We selected 90-yr sliding windows with a 30-yr interval and calculated the ratio of ENSO amplitude between all the possible pairs of windows. The change in ENSO amplitude under global warming is significant in a model if the ratio of the standard deviation in the twenty-first century to that in the twentieth century exceeds the 10%–90% range of the ratio in the control run.

To investigate the SST warming pattern effect on the atmospheric response of ENSO to global warming and related intermodel uncertainties, we analyze three sets of atmospheric experiments following the Atmospheric Model Intercomparison Project (AMIP) protocol from the CMIP5 archive (Gates et al. 1999). The three experiments are forced by the observed SST field for 1979–2008 (control run, known in CMIP5 terminology as the amip run), plus a spatially uniform SST increase of 4 K over the globe (the amip4K run in CMIP5), and a patterned SST increase [derived from CMIP3 multimodel ensemble mean of the quadruple CO_2 (from 1% to 4 times) simulations, called the amipFuture run]. The three experiments share the same interannual SST anomalies, and differ only in SST climatology. A total of 11 AGCMs are available for this study (Table 2).

To further demonstrate the increased convective variability under global warming more clearly, we examine the rainfall response to a composite of strong El Niño events under different climatological SST fields using the Community Atmosphere Model, version 4

TABLE 2. The 11 AMIP models used in this study.

Model name	Institute (country)
BCC_CSM1.1	Beijing Climate Center, China Meteorological Administration (China)
CanAM4	Canadian Centre for Climate Modelling and Analysis (Canada)
CCSM4	National Center for Atmospheric Research (United States)
CNRM-CM5	Centre National de Recherches Météorologiques (France)
HadGEM2-A	Met Office Hadley Centre (United Kingdom)
IPSL-CM5A-LR	L'Institut Pierre-Simon Laplace (France)
IPSL-CM5B-LR	L'Institut Pierre-Simon Laplace (France)
MIROC5	University of Tokyo, Atmosphere and Ocean Research Institute, National Institute for Environmental Studies, and Japan Agency for Marine-Earth Science and Technology (Japan)
MPI-ESM-LR	Max Planck Institute for Meteorology (Germany)
MPI-ESM-MR	Max Planck Institute for Meteorology (Germany)
MRI-CGCM3	Meteorological Research Institute (Japan)

(CAM4; Neale et al. 2010). An El Niño composite of SST anomalies, which evolves from January of the El Niño developing year to December of the decay year, is added globally to the climatological SST to force CAM4 model. We have performed three pairs of integrations analogous to the amip, amip4K, and amipFuture experiments from CMIP5: 1) present-day climatology with and without composite El Niño SST anomalies; 2) the same as integration 1 but for a mean state of the present-day SST climatology plus a spatially uniform SST increase (SUSI) of 2.5 K; and 3) the same as integration 1 but for a mean state of the present-day climatology plus a spatially patterned SST increase (SPSI) over the globe. The SPSI is derived from the CCSM4 as the 2081–2100 mean of the RCP8.5 run minus the 1986–2005 mean of the historical run. Each set of experiments has 20 members, each member lasting 2 years from January of the El Niño developing year to December of the following year. Detailed information about the AMIP and CAM4 experiments can be found in Zhou et al. (2014).

In this study, the SST and rainfall averaged in the eastern equatorial Pacific (Niño-3; 5°N–5°S, 90°–150°W) are referred to as the ENSO SST and rainfall indices, respectively. The zonal wind in the central equatorial Pacific (Niño-4; 5°N–5°S, 160°E–150°W) and difference of sea level pressure between the eastern (5°N–5°S, 130°–80°W) and western (5°N–5°S, 90°–140°E) equatorial Pacific are defined as the ENSO zonal wind and equatorial Southern Oscillation (eqSO) indices, respectively. To focus on the interannual variability, we calculate the anomalies by performing a 3-month running average to reduce intraseasonal variability, and then subtracting a 9-yr running mean to remove decadal and longer variations in CMIP5 output. The change in amplitudes of SST, rainfall, eqSO, and zonal wind indices is represented by the ratio of the standard deviation in the twenty-first century to that in the twentieth century. We also calculate the total rainfall over the Niño-3 region ($P_{\text{Niño-3}}$) to examine the SST threshold for convection, which is important for the ENSO amplitude change under global warming.

3. ENSO changes and intermodel uncertainty

Under global warming, the ENSO amplitude in SST changes little in the multimodel ensemble mean, with large diversity among models (Collins et al. 2010; Cai et al. 2015a). Figure 1a shows the amplitude changes in Niño-3 SST, Niño-3 rainfall, eqSO index (eqSOI), and Niño-4 zonal wind, as represented by the twenty-first to twentieth century ratio of the standard deviation. The amplitudes in SST and eqSOI remain nearly unchanged in CMIP5 ensemble-mean projections, but with large intermodel uncertainties. By contrast, amplitudes in rainfall and zonal wind significantly increase as reported in previous studies. Specifically, the amplitude in rainfall increases by 30% in the ensemble mean, albeit with a huge spread among models. The intermodel variability is highly correlated among different measures of ENSO amplitude (Figs. 1b–d). Specifically, the change in SST amplitude is correlated with the changes in eqSOI, rainfall, and equatorial zonal wind indices, at $r = 0.84$, 0.92, and 0.88, respectively. The high correlations among the ocean–atmospheric measures of amplitude in SST, rainfall, eqSOI, and zonal wind indices are indicative of the Bjerknes (1969) feedback in the equatorial Pacific.

a. Role of relative SST

ENSO induces the anomalous tropical convection over the central and eastern equatorial Pacific. Since the SST threshold for convection can be approximated by the tropical-mean SST, the relative SST change to the tropical mean warming shows a better correlation with changes in tropical convection and tropical cyclone frequency than the absolute SST in a changing climate (Johnson and Xie 2010; Vecchi and Soden 2007b; Lin

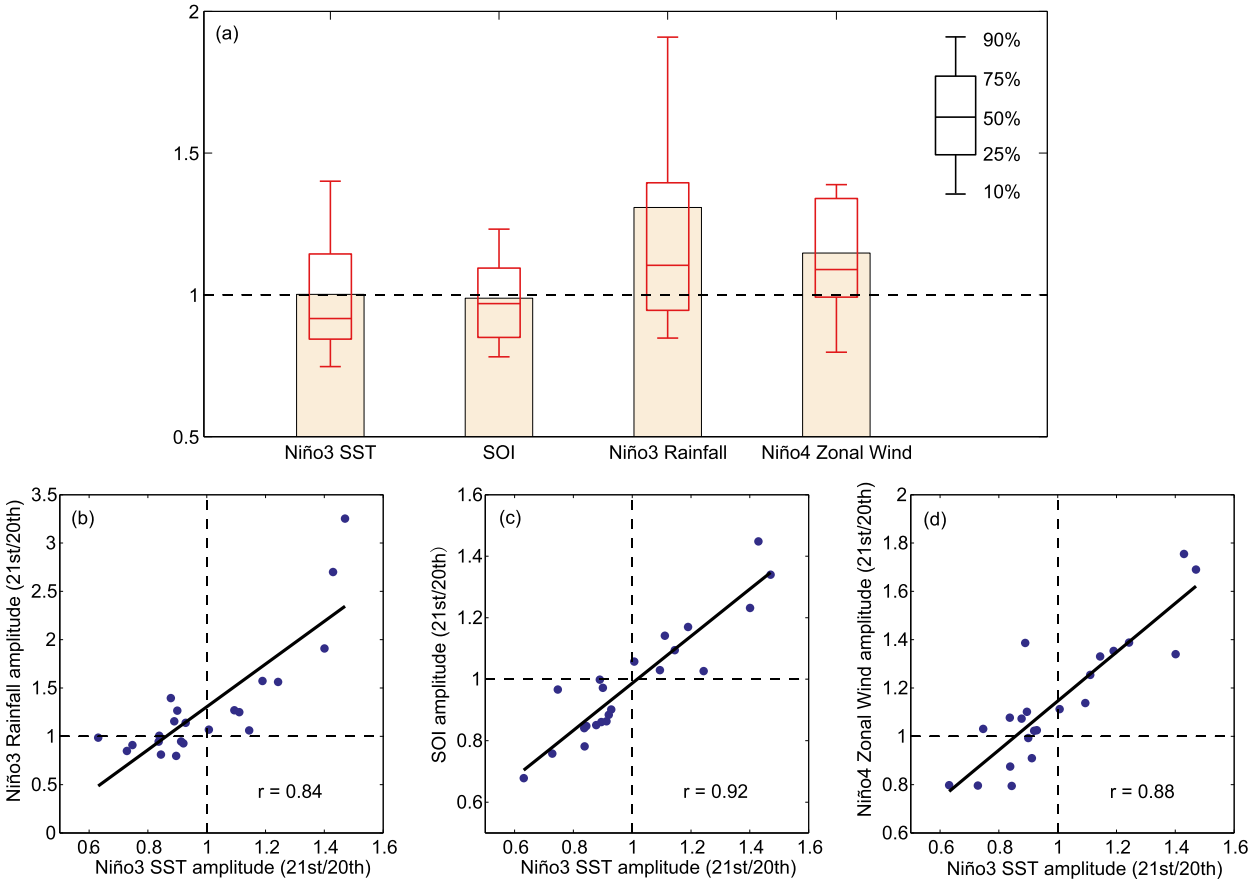

FIG. 1. (a) Twenty-first to twentieth century ratio of interannual standard deviation for Niño-3 SST ($T_{\text{Niño-3}}$), Southern Oscillation index, Niño-3 rainfall ($P_{\text{Niño-3}}$), and Niño-4 zonal wind. Black boxes are for the CMIP5 multimodel ensemble mean while box-and-whisker plots show the 10th, 25th, 50th, 75th, and 90th percentiles, representing the intermodel variability. Also shown are scatterplots of twenty-first to twentieth century ratios of interannual standard deviation for $T_{\text{Niño-3}}$ vs (b) $P_{\text{Niño-3}}$, (c) eqSOI, and (d) Niño-4 zonal wind. The solid line in (b)–(d) denotes the linear regression.

et al. 2015). Here the relative SST in the Niño-3 region ($T^*_{\text{Niño-3}}$) is defined as $T^*_{\text{Niño-3}} = T_{\text{Niño-3}} - T_{\text{tropical-mean}}$, where $T_{\text{Niño-3}}$ is SST in the Niño-3 region and $T_{\text{tropical-mean}}$ is the tropical mean over 20°S–20°N. Figures 2a and 2b show the scatter diagrams of $T^*_{\text{Niño-3}}$ and $P_{\text{Niño-3}}$ for November–January (NDJ) in present and future climates in 22 CMIP5 models. The T^*–P slope differs markedly between the positive and negative $T^*_{\text{Niño-3}}$, indicating that the tropical mean SST is a good approximation for the SST threshold for convection (Johnson and Xie 2010): When $T_{\text{Niño-3}}$ exceeds $T_{\text{tropical-mean}}$ ($T^*_{\text{Niño-3}} > 0$), rainfall increases more rapidly with increasing $T^*_{\text{Niño-3}}$ than for $T^*_{\text{Niño-3}} < 0$.

The El Niño–like warming in climatology appears in the ensemble mean and most CMIP5 models (Fig. 3). It is conceivable that the enhanced warming in the eastern equatorial Pacific increases the number of years when SST exceeds the convective threshold in a warmer climate (Fig. 2). Consistently, the frequency of extreme El Niño events as defined in Cai et al. (2014) nearly doubles in the twenty-first century. The locally enhanced mean warming in the eastern equatorial Pacific shifts the probability density distribution of $T^*_{\text{Niño}}$ toward the positive side in the future warmer climate (Fig. 4), thereby intensifying local convection.

b. *SST warming pattern effect on intermodel uncertainty*

Among 22 CMIP5 models, tropical SST warming pattern in the mean shows considerable variation (Fig. 3). Several models (such as FGOALS-g2, GFDL-ESM2M, INM-CM4.0, and NorESM1-M) even produce La Niña–like patterns with reduced warming in the eastern compared to the western equatorial Pacific. Likewise the changes in rainfall and the T^*–P relationship under global warming show large diversity among the models. Here we select four models (MRI-CGCM3, MIROC5, CanESM2, and MPI-ESM-MR) with the

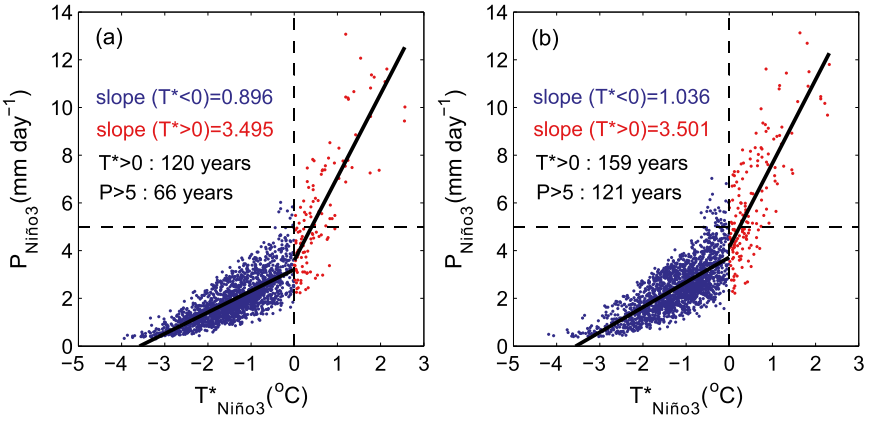

FIG. 2. Scatterplots of $T^*_{\text{Niño-3}}$ (°C) and $P_{\text{Niño-3}}$ (mm day^{-1}) for NDJ during (a) 1911–2000 and (b) 2006–95 from 22 CMIP5 models. The solid lines denote the linear regressions for positive and negative $T^*_{\text{Niño-3}}$, separately.

largest $T^*_{\text{Niño-3}}$ increase and an El Niño–like mean warming pattern, and another four models (FGOALS-g2, NorESM1-M, GFDL-ESM2M, and INM-CM4.0) with decreased $T^*_{\text{Niño-3}}$ and a La Niña–like warming pattern. Although the $T^*_{\text{Niño-3}}$–$P_{\text{Niño-3}}$ relationship varies among the models (Cai et al. 2014), the different response of rainfall variability between the two groups illustrates the importance of the warming pattern (Fig. 5). In the models with an El Niño–like warming pattern, Niño-3 SST exceeds the convective threshold ($T^*_{\text{Niño-3}} > 0$) more frequently in the warmer climate. As a result, the standard deviation of $P_{\text{Niño-3}}$ increases substantially. In comparison, in the models with a La Niña–like warming, there are fewer events exceeding the convective threshold in the warmer climate, with little changes in $P_{\text{Niño-3}}$ and its variability.

The above comparison between two model groups suggests the possibility that the intermodel diversity in ENSO amplitude change comes from that in SST warming pattern. To examine this relationship, an intermodel empirical orthogonal function (EOF) is performed on mean SST warming to extract the diversity of the warming pattern (Fig. 6). There is large intermodel diversity in tropical mean warming magnitude, which could influence the EOF results substantially. Therefore, the SST changes are normalized by the tropical mean (20°S–20°N) in each model before the EOF analysis. The leading mode shows an enhanced equatorial warming in the central and eastern Pacific (Fig. 6a). A model with a positive principal component (PC) value tends to show an El Niño–like enhanced warming in the tropical Pacific, while a model with a negative PC value shows a La Niña–like warming pattern. We find that models with positive PC1 (i.e., an El Niño–like warming pattern) have a larger positive change of $T^*_{\text{Niño-3}}$ ($\Delta T^*_{\text{Niño-3}}$), suggesting that $T^*_{\text{Niño-3}}$ is a good indicator of intermodel uncertainty in the Pacific warming pattern (Fig. 7a). Similarly, the atmospheric change such as percentage rainfall and zonal circulation are also significant correlated with the PC1, at $r = 0.76$ and 0.77, respectively (Figs. 7b,c). These intermodel variabilities in mean state changes follow the Bjerknes feedback and the warmer-get-wetter mechanism (Xie et al. 2010; Ma and Xie 2013).

Among the 22 CMIP5 models examined here, the intermodel diversity in ENSO SST amplitude change is highly correlated with that in the relative mean warming $\Delta T^*_{\text{Niño-3}}$ at $r = 0.55$ (Fig. 8c). The intermodel variability in $\Delta T^*_{\text{Niño-3}}$ is also closely related to amplitude changes in rainfall and zonal wind indices (Figs. 8a,b). Recent studies corroborate the intermodel relationship between zonal wind feedback and SST amplitude (An and Choi 2015; Rashid et al. 2016). Thus our results show that it is the warming pattern that affects the wind response via convective feedback and determines ENSO SST amplitude. Note that the correlation increases for $\Delta T^*_{\text{Niño-3}} > 0$ with $r = 0.65$ (although the correlation change does not exceed the 95% significance level): the enhanced convective feedback amplifies ENSO, while a reduced $T^*_{\text{Niño-3}}$ has little effect on atmospheric convection and circulation. If an El Niño–like warming pattern with an equatorial peak is projected by a model, the reduced barrier to the convective threshold intensifies atmospheric response, amplifying the ENSO variability in SST in a warmer climate. While confirming that ENSO SST amplitude change is highly uncertain among models (Collins et al. 2010; Cai et al. 2015a), our results take one step further by showing that this intermodel uncertainty is related to that in the projected mean SST warming pattern.

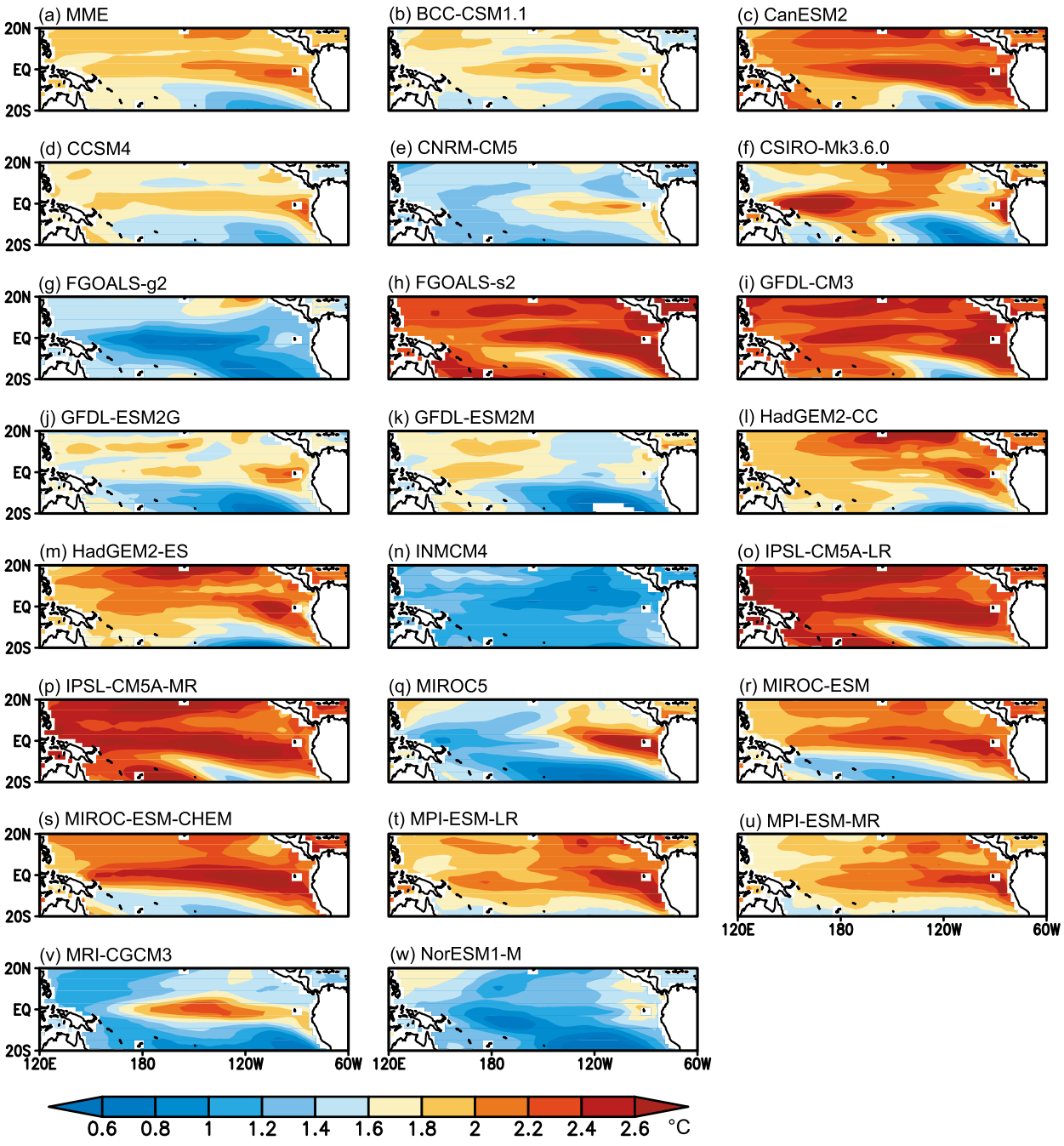

FIG. 3. SST changes (°C) under global warming for (a) MME and (b)–(w) 22 CMIP5 models in the tropical Pacific. The warming shown in each model is significant, reaching 99% significance level based on the Student's *t* test.

Centennial difference in ENSO SST amplitude includes internal modulations (Wittenberg 2009; Ogata et al. 2013; Wittenberg et al. 2014). This natural low-frequency ENSO modulation is an important source of uncertainty in projecting ENSO amplitude change under global warming (Stevenson 2012). We have evaluated the range of internal modulations in preindustrial control simulations. About half of the models show significant forced changes in ENSO amplitude in RCP8.5 (Fig. 9a). By contrast, $\Delta T^*_{\text{Niño-3}}$ is beyond the range of internal variations in most (20 out of 22) models, indicating a significant change in the mean state (Fig. 9b). Furthermore, the intermodel relationship between changes in ENSO SST amplitude

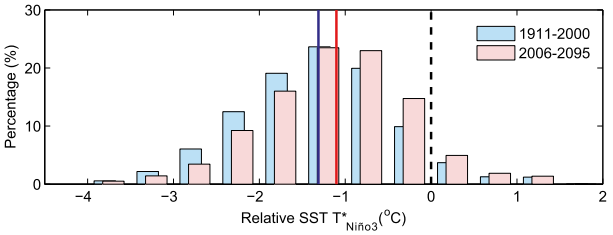

FIG. 4. The MME percentage histogram of $T^*_{\text{Niño-3}}$ (°C) during 1911–2000 (blue bars) and 2006–95 (red bars) in 22 CMIP5 models. The solid lines denote the MME climatological $T^*_{\text{Niño-3}}$ during 1911–2000 (blue) and 2006–95 (red), respectively.

and mean SST warming pattern is much higher among models with a significant change in ENSO amplitude ($r = 0.63$, filled circle) than those without ($r = 0.35$, open circle) (Fig. 8c). Thus, the intermodel relationship between ENSO SST amplitude change and mean SST warming pattern probably reflects the response to anthropogenic forcing, rather than due to internal variability.

Considering that the internal variability of ENSO amplitude potentially influences the future projection of ENSO change under global warming, a multimember analysis for each model is desirable. However, more than half of the 22 models have only one member run for historical or RCP8.5 simulation, limiting the assessment of the uncertainty in ENSO change due to internal variability.

4. AGCM experiments

In this section, we turn to atmospheric model experiments forced by observed SST variability to further illustrate the effect of spatially patterned warming on convection. In the amipFuture and SPSI experiments, the SST warming shows an El Niño–like pattern [see Fig. 1 in Zhou et al. (2014)], similar to the CMIP5 ensemble mean (Fig. 3a). Comparison between the patterned warming and uniform warming (amip4k and SUSI) experiments can isolate the effect of warming pattern on the changes in ENSO-induced atmospheric variability.

Although the SST anomalies of ENSO are identical in all the AMIP simulations, rainfall and zonal wind anomalies intensify over the central and eastern equatorial Pacific in the spatially patterned warming experiments compared to uniform warming experiments, following the above-mentioned T^*–P relationship. Figure 10a shows the scatterplot between $T^*_{\text{Niño-3}}$ and $P_{\text{Niño-3}}$ during six El Niño events (1982/83, 1987/88, 1991/92, 1997/98, 2002/03, and 2006/07) in amip, amip4k, and amipFuture. For the four moderate El Niño (1987/88, 1991/92, 2002/03, and 2006/07) events, when the Niño-3 SST does not reach the convection threshold ($T^*_{\text{Niño-3}} < 0$), the rainfall anomalies are weak. In comparison, during the 1982/83 and 1997/98 El Niño events Niño-3 SST exceeds the convective threshold ($T^*_{\text{Niño-3}} > 0$), and rainfall increases greatly compared to the climatology. Since $T^*_{\text{Niño-3}}$ is higher in amipFuture than amip with an El Niño–like warming pattern, $P_{\text{Niño-3}}$ is much larger in amipFuture than in amip, with the difference exceeding 99% significance level based on the Student's t test. With the uniform warming (green symbols), by contrast, $T^*_{\text{Niño-3}}$ in amip4k experiment does not change much compared with amip. As a result, the El Niño rainfall changes much less in amip4k than that in amipFuture (the difference exceeds 99% significance level based on the Student's t test).

The enhanced atmospheric responses to El Niño under patterned warming are further supported by the regressions of equatorial rainfall and zonal wind to interannual $T_{\text{Niño-3}}$ anomalies in three sets of AMIP experiments (Figs. 10c,e). In the amipFuture the ENSO rainfall increases over the central and eastern Pacific with enhanced westerly wind anomalies along the equator, consistent with the eastward shifts of ENSO-induced atmospheric variability as reported previously (Power et al. 2013; Chung et al. 2014; Zhou et al. 2014).

We obtained similar results in three sets of CAM4 experiments regarding the response of strong El Niño events. Compared with El Niño under the present-day climatology and SUSI, Niño-3 rainfall strengthens as $T^*_{\text{Niño-3}}$ increases in SPSI experiment (Fig. 10b). The anomalies of rainfall and zonal wind along the equator both shift eastward in SPSI (Figs. 10d,f). Since CAM4 experiments are forced by an El Niño composite, we examine anomalies in Figs. 10d and 10f. By contrast, the changes in El Niño–induced rainfall and zonal wind are much less in SUSI, supporting the idea that the amplification of atmospheric anomalies during El Niño mainly originates from the El Niño–like mean warming pattern and reduced convection barrier in the eastern equatorial Pacific. The intensification and eastward shift of zonal wind anomalies act to intensify ENSO SST variability in coupled models (An and Choi 2015). Indeed, in the models with an El Niño–like warming pattern, the rainfall and zonal wind anomalies increase along the equator, reflecting the effect of enhanced convective response (Figs. 11a,b). By contrast, rainfall and zonal wind anomalies change little along the equator in the models with La Niña–like warming pattern (Figs. 11c,d). The distinct changes in ENSO rainfall and zonal wind between the two model groups illustrate the importance

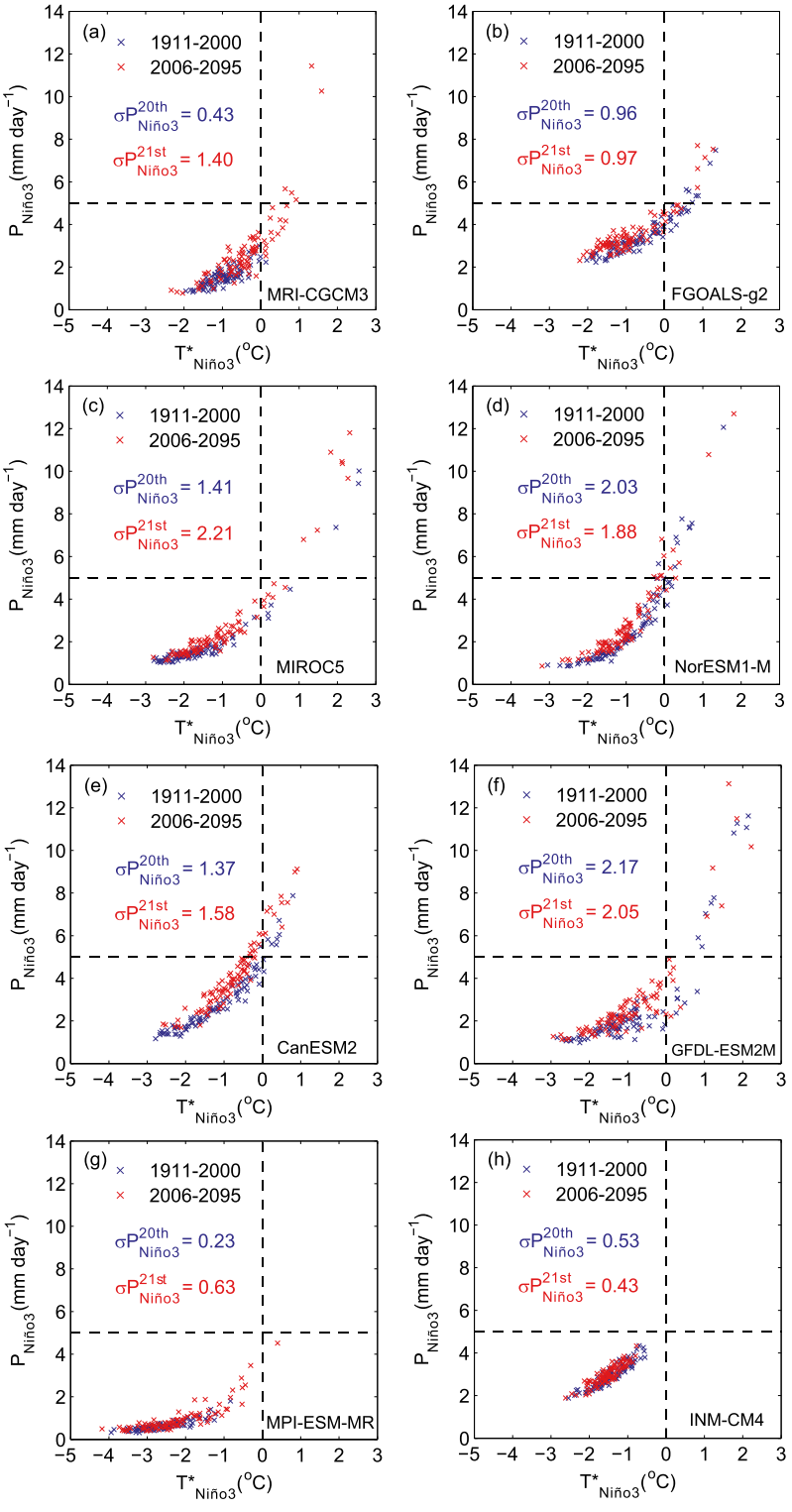

FIG. 5. Scatterplots of $T^{*}_{\text{Niño-3}}$ (°C) and $P_{\text{Niño-3}}$ (mm day^{-1}) for NDJ during 1911–2000 (blue cross) and 2006–95 (red cross) in four models with El Niño–like warming: (a) MRI-CGCM3, (c) MIROC5, (e) CanESM2, and (g) MPI-ESM-MR. (b),(d),(f),(h) As in (a),(c),(e),(g), but for four models (FGOALS-g2, NorESM1-M, GFDL-ESM2M, and INM-CM4.0, respectively) with La Niña–like warming.

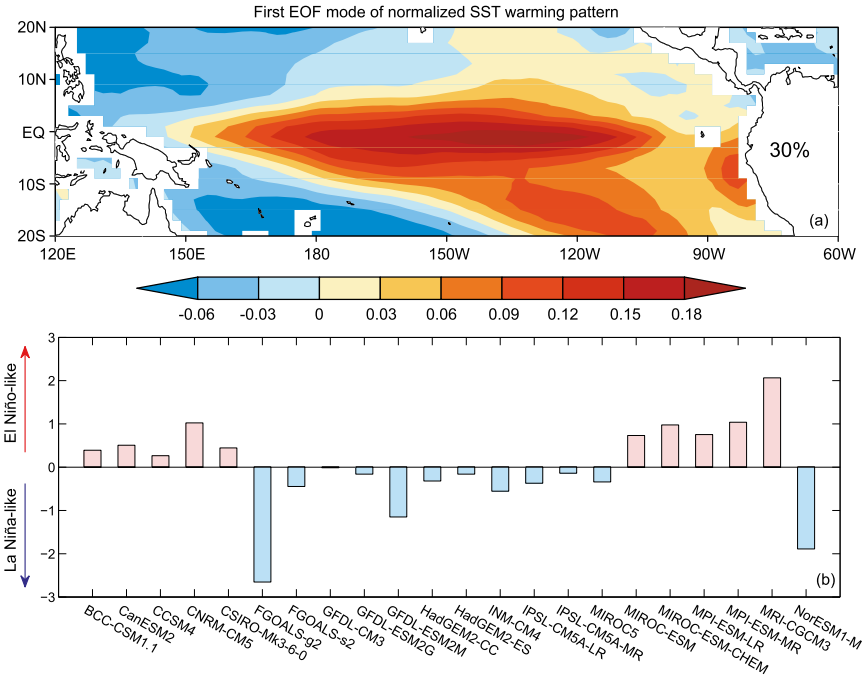

FIG. 6. (a) The first EOF mode of intermodel spread in SST change (°C) in CMIP5 models. The SST change is normalized (divided) by the tropical mean SST warming in each model to isolate the effect of warming pattern. (b) The intermodel principal component.

of SST warming pattern on change in atmospheric response to ENSO, and hence in ENSO SST amplitude. Note that the mean warming pattern may also influence ENSO amplitude via other processes, such as oceanic feedback (Kim et al. 2014). This needs to be investigated in future studies.

Figure 12 compares the ensemble mean normalized change in $P_{\text{Niño-3}}$ variability between the CMIP5 and AMIP ensembles. The comparison enables us to evaluate the contribution of the intermodel uncertainty in SST warming pattern to the uncertainty in changes of ENSO rainfall variability. To compare the results in different model scenarios, the changes in $P_{\text{Niño-3}}$ amplitude are normalized by the tropical mean SST warming. In the ensemble mean, $P_{\text{Niño-3}}$ variability increases much more in CMIP5 (17.8%) and patterned warming experiments (amipFuture; 20.3%) than that in uniform warming AMIP experiments (amip4k; 4.5%). Furthermore, changes in $P_{\text{Niño-3}}$ amplitude shows a larger intermodel uncertainty in the CMIP5 ensemble than in AMIP ensembles (see the box-and-whisker plot in Fig. 12) because of the

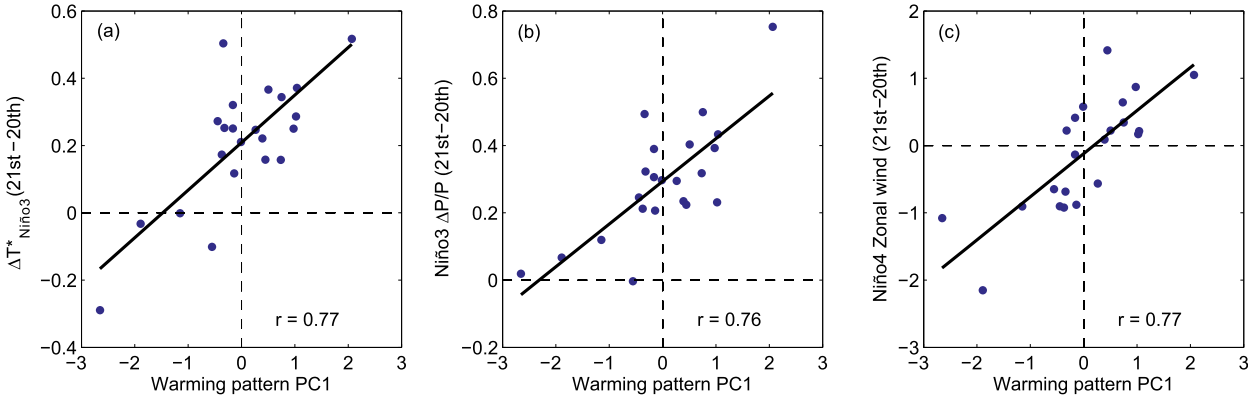

FIG. 7. The scatterplots of PC1 for intermodel SST spread with the changes in mean (a) $T^*_{\text{Niño-3}}$, (b) percentage $P_{\text{Niño-3}}$, and (c) Niño-4 zonal wind from 1911–2000 to 2006–95. The solid line denotes the linear regression.

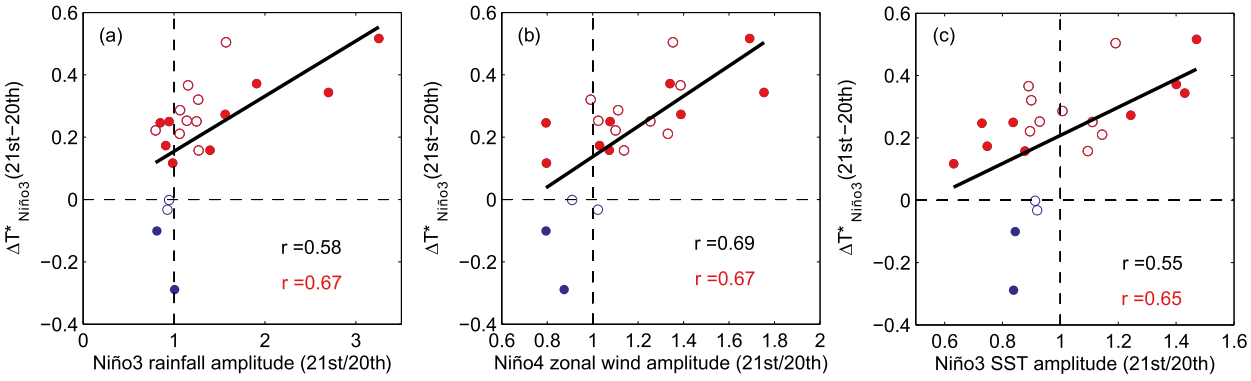

FIG. 8. Intermodel scatterplots between $\Delta T^*_{\text{Niño-3}}$ (°C) and the twenty-first to twentieth century ratio of standard deviation for (a) $P_{\text{Niño-3}}$, (b) Niño-4 zonal wind, and (c) $T_{\text{Niño-3}}$. The filled (open) circles denote models in which ENSO SST amplitude change significantly (insignificantly) compared with the preindustrial control run. The circles in red denote the model in which $\Delta T^*_{\text{Niño-3}}$ is positive. The solid line denotes the linear regression. The intermodel correlations for all models and models with positive $\Delta T^*_{\text{Niño-3}}$ are shown in black and red, respectively.

intermodel variations in the mean SST warming pattern in CMIP5. To verify the robustness of the result, we select a subset of 11 coupled models that share the same atmospheric models that form the AMIP ensemble. The intermodel uncertainty is still much larger than in the AMIP ensemble (the box-and-whisker plot of the second column in Fig. 12). To the extent that changes in ENSO SST anomaly pattern in response to global warming are small in CMIP5 simulations [Figs. 2a,b of Power et al. (2013)], AGCM results corroborate the importance of the spatial pattern of mean SST warming for ENSO amplitude change under global warming.

5. Summary and discussion

The change of ENSO SST amplitude shows large intermodel uncertainty in CMIP5 simulations. We show that this uncertainty is closely related to the spatial pattern of mean SST warming in the tropical Pacific. A model with enhanced warming in the eastern equatorial Pacific brings SST close to the convective threshold,

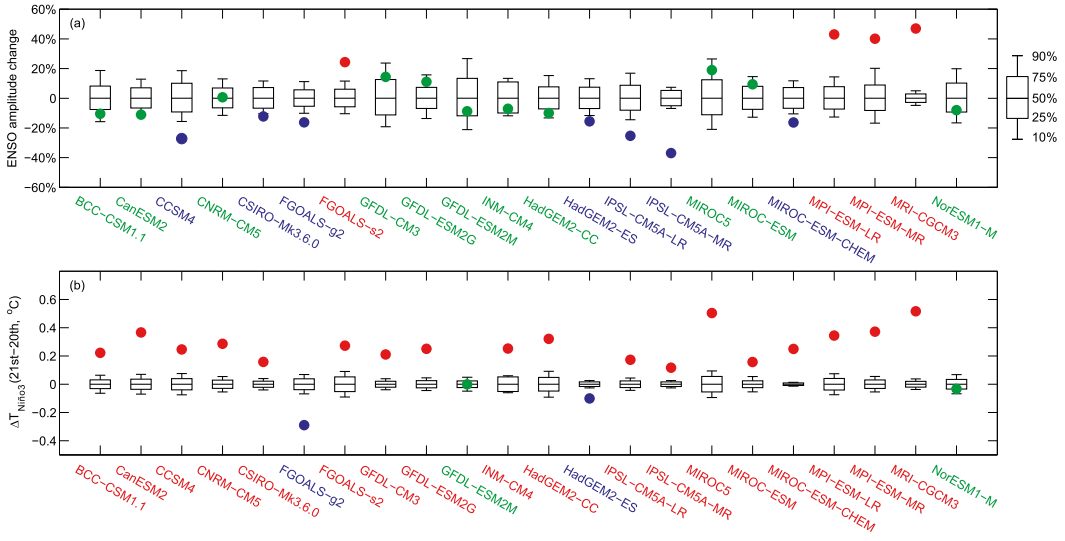

FIG. 9. (a) The percentage changes in $T_{\text{Niño-3}}$ standard deviation in 22 CMIP5 models compared with the low-frequency modulation of ENSO SST amplitude. The filled dots represent ENSO SST amplitude change under global warming, while box-and-whisker plots represent the range of ENSO natural modulation based on the nearest rank. (b) As in (a), but for $\Delta T^*_{\text{Niño-3}}$. Significant increase, significant decrease, and insignificant projected change with model name are shown in red, blue, and green, respectively.

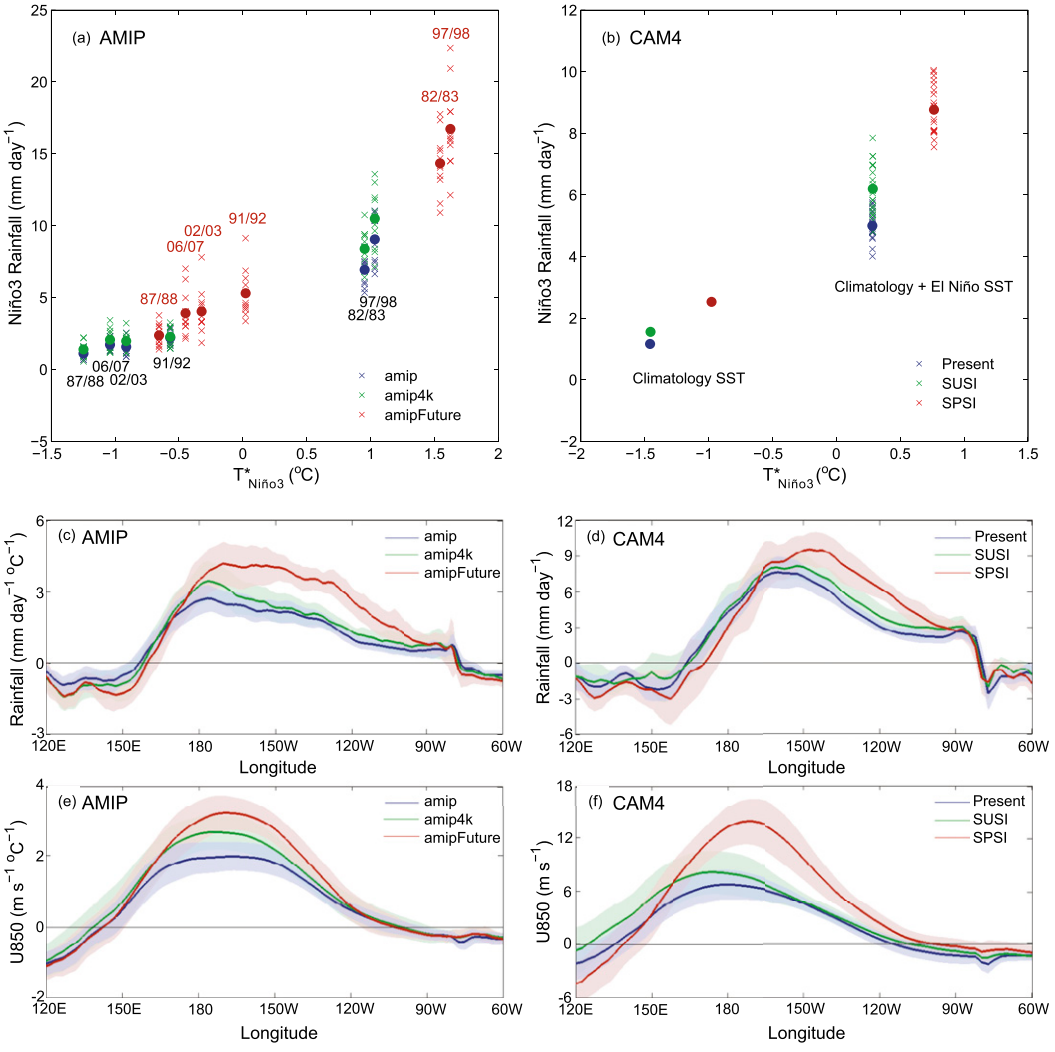

FIG. 10. Scatterplots of $T^*_{\text{Niño-3}}$ (°C) and $P_{\text{Niño-3}}$ (mm day^{-1}) for NDJ during El Niño events in (a) AMIP and (b) CAM4 experiments. The dot denotes the multimodel ensemble mean value while the cross denotes the result from an individual member. Also shown is the ensemble mean regression of (c) rainfall (mm day^{-1} °C^{-1}) and (e) zonal wind (m s^{-1} °C^{-1}) along the equator (averaged over 5°S–5°N) upon $T_{\text{Niño-3}}$ anomalies during NDJ in three sets of AMIP experiments. The shading shows one standard deviation of intermodel variability. (d),(f) As in (c),(e), but for anomalies in CAM4 experiments.

amplifying the convective response and increasing the ENSO SST amplitude. The changes in ENSO-induced atmospheric variability are further investigated based on the SST-forced AGCM experiments. Forced by the spatially patterned mean SST warming derived from coupled model projections, the rainfall anomalies of El Niño intensify and shift eastward in the eastern equatorial Pacific. In addition, the intermodel diversity in changes in ENSO rainfall among AGCMs is much smaller than among corresponding coupled models, indicating that the regional pattern of SST warming in the tropical Pacific is the main source of uncertainty in future projections of ENSO variability.

A paradox has been that the intensification of atmospheric anomalies of El Niño is robust among models despite a lack of consistency in the projection of SST amplitude change in the CMIP ensemble. The amipFuture experiments (Fig. 12) show that even if the ENSO SST anomalies do not change at all, interannual atmospheric anomalies still amplify in a warmer climate (Power et al. 2013) on the condition of an enhanced mean warming in the equatorial Pacific. This condition is corroborated by the amip4k experiment: with spatially uniform warming, the change in atmospheric anomalies of ENSO is modest. A long-standing issue of ENSO projections is the large intermodel spread in SST variance change. We show that

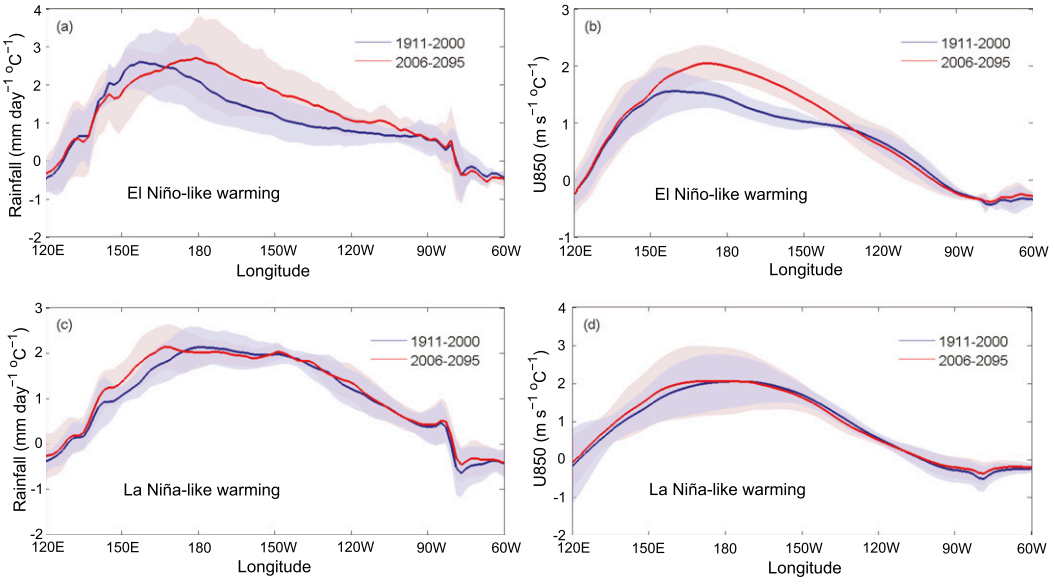

FIG. 11. The ensemble mean regressions of (a) rainfall (mm day^{-1} °C^{-1}) and (b) zonal wind (m s^{-1} °C^{-1}) along the equator (averaged over 5°S–5°N) upon $T_{\text{Niño-3}}$ anomalies during NDJ in four models (MRI-CGCM3, MIROC5, CanESM2, and MPI-ESM-MR) with El Niño–like warming pattern. (c),(d) As in (a),(b), but for four models (FGOALS-g2, NorESM1-M, GFDL-ESM2M, and INM-CM4.0) with La Niña–like warming pattern.

this intermodel spread is correlated with that in the mean relative SST change in Niño-3 region, especially among models with positive $\Delta T^*_{\text{Niño-3}}$. This suggests that changes in convective feedback in the central and eastern Pacific are important for SST variance. It is interesting to note, however, that ENSO SST amplitude decreases at the intersect of $T^*_{\text{Niño-3}} = 0$ (Fig. 8c), implying that other feedbacks are to weaken ENSO under global warming and counteract the effect of increased convective feedback in the ensemble mean. For example, oceanic processes, which are beyond the scope of this study, play an important role in ENSO changes in future projections (Kim et al. 2014; An and Choi 2015).

Previous attempts to explain the large intermodel uncertainty in projected change in ENSO amplitude have met with limited success. The intermodel correlations of ENSO SST amplitude change with changes of absolute Niño-3 SST and meridional SST gradient [defined in Cai et al. (2014)] are both insignificant, at $r = 0.16$ and -0.03, respectively. A recent study reported a poor intermodel correlation between the projected changes in ENSO SST amplitude and mean rainfall in the Niño-3 region under global warming (Watanabe et al. 2012). While we are able to reproduce this result (Fig. 13a), here we identified a crucial connection to the mean warming pattern instead. The significant intermodel correlation between ENSO SST amplitude change and relative SST warming for $\Delta T^*_{\text{Niño-3}} > 0$ indicates that the mean warming pattern is more fundamental than the mean rainfall change in predicting changes in atmospheric amplitude (cf. Figs. 8 and 13). For the same reason, the ocean warming pattern effect is stronger in El Niño events when eastern Pacific SST may exceed the convective threshold than in La Niña events. This causes an asymmetry in ENSO rainfall response to global warming as reported earlier elsewhere (Cai et al. 2014, 2015b; Chung et al. 2014; Chung and Power 2014).

This study revealed a robust relationship between the changes in ENSO variability and the tropical Pacific mean state. This suggests that better understanding the

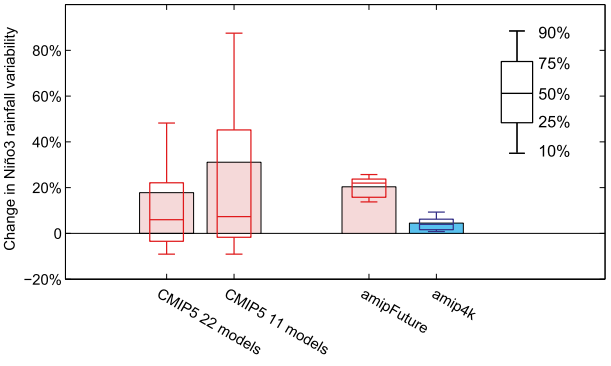

FIG. 12. The multimodel ensemble mean percentage changes in $P_{\text{Niño-3}}$ standard deviation. The box-and-whisker plot represents intermodel variability. To compare the results among different models, all the results are normalized by the tropical mean SST warming. The AMIP amipFuture and amip4k experiments include 11 models, whereas the full CMIP5 ensemble includes 22 models. A CMIP5 subensemble includes the same 11 models as the AMIP ensembles. The spread among the 11-model CMIP5 ensemble is much larger than that in AMIP ensembles.

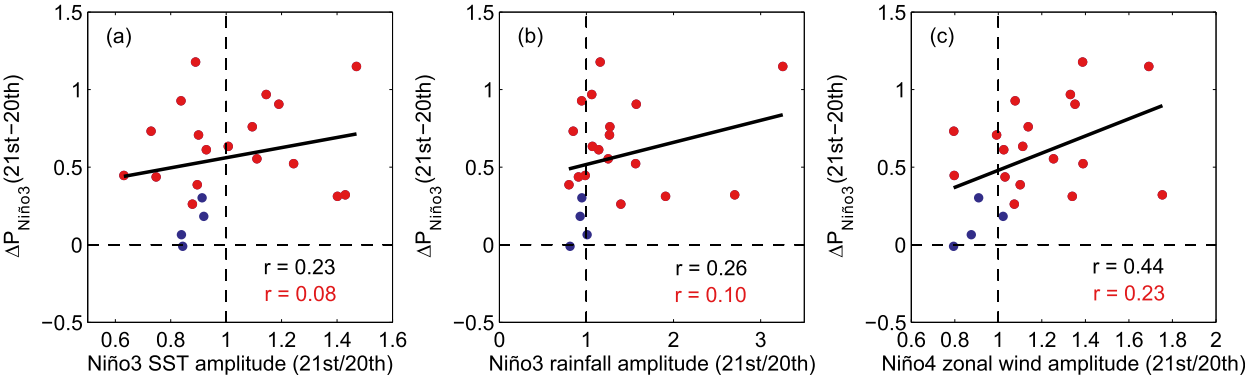

FIG. 13. The intermodel scatterplots of the ENSO amplitude ratios between 1911–2000 and 2006–95 with $\Delta P_{\text{Niño-3}}$ (mm day^{-1}): (a) Niño-3 SST, (b) Niño-3 rainfall, and (c) Niño-4 zonal wind. The red dots denote models with positive $\Delta T^*_{\text{Niño-3}}$. The solid line denotes the linear regression.

mean SST warming pattern helps reduce the uncertainty in projecting ENSO amplitude change. The uncertainty in SST warming pattern among coupled models appears related to the biases in the mean state over the tropical Pacific. Specifically, a recent study revealed that the simulation of the equatorial cold tongue could influence the warming pattern in the tropical Pacific in climate models (Li et al. 2016). Li et al. (2016) suggested that the bias of an excessive equatorial cold tongue suppresses and weakens the negative cloud–SST feedback over the western tropical Pacific, resulting in an excessive warming in the warm pool region and spurious La Niña–like warming pattern. Correcting the cold tongue bias by using an ''observational constraint'' method leads to a more robust projection of an El Niño–like warming pattern over the equatorial Pacific (Huang and Ying 2015; Li et al. 2016). From our results this implies a likely intensification in SST amplitude of ENSO. We will investigate this hypothesis in the future. Uncertainties are large regarding the spatial pattern of historical SST warming over the tropical Pacific (Vecchi et al. 2008; Tokinaga et al. 2012), partly because of internal variability (Kosaka and Xie 2013; England et al. 2014). Our results (Fig. 9) suggest that the mean warming pattern is likely to emerge earlier than ENSO variance change. Hence, the monitoring and detection of the equatorial mean state change provide skill in predicting ENSO change as climate warms.

Acknowledgments. We would like to acknowledge helpful suggestions from three anonymous reviewers. We acknowledge the World Climate Research Programme's Working Group on Coupled Modelling, which is responsible for CMIP, and we thank the climate modeling groups (listed in Tables 1 and 2 of this paper) for producing and making available their model output. For CMIP the U.S. Department of Energy's Program for Climate Model Diagnosis and Intercomparison provides coordinating support and led development of software infrastructure in partnership with the Global Organization for Earth System Science Portals. This work was supported by the National Basic Research Program of China (2012CB955600), the National Natural Science Foundation of China (41476003), NSFC-Shandong Joint Fund for Marine Science Research Centers (U1406401), and the U.S. National Science Foundation (1305719 and 1249145).

REFERENCES

An, S.-I., and J. Choi, 2015: Why the twenty-first century tropical Pacific trend pattern cannot significantly influence ENSO amplitude? *Climate Dyn.*, **44**, 133–146, doi:10.1007/s00382-014-2233-2.

Bjerknes, J., 1969: Atmospheric teleconnections from the equatorial Pacific. *Mon. Wea. Rev.*, **97**, 163–172, doi:10.1175/1520-0493(1969)097<0163:ATFTEP>2.3.CO;2.

Cai, W., and Coauthors, 2014: Increasing frequency of extreme El Niño events due to greenhouse warming. *Nat. Climate Change*, **4**, 111–116, doi:10.1038/nclimate2100.

——, and Coauthors, 2015a: ENSO and greenhouse warming. *Nat. Climate Change*, **5**, 849–859, doi:10.1038/nclimate2743.

——, and Coauthors, 2015b: Increased frequency of extreme La Niña events under greenhouse warming. *Nat. Climate Change*, **5**, 132–137, doi:10.1038/nclimate2492.

Cane, M. A., A. C. Clement, A. Kaplan, Y. Kushnir, D. Pozdnyakov, R. Seager, S. E. Zebiak, and R. Murtugudde, 1997: Twentieth-century sea surface temperature trends. *Science*, **275**, 957–960, doi:10.1126/science.275.5302.957.

Chadwick, R., I. Boutle, and G. Martin, 2013: Spatial patterns of precipitation change in CMIP5: Why the rich do not get richer in the tropics. *J. Climate*, **26**, 3803–3822, doi:10.1175/JCLI-D-12-00543.1.

Chung, C. T. Y., and S. B. Power, 2014: Precipitation response to La Niña and global warming in the Indo-Pacific. *Climate Dyn.*, **43**, 3293–3307, doi:10.1007/s00382-014-2105-9.

——, ——, J. M. Arblaster, H. A. Rashid, and G. L. Roff, 2014: Nonlinear precipitation response to El Niño and global

warming in the Indo-Pacific. *Climate Dyn.*, **42**, 1837–1856, doi:10.1007/s00382-013-1892-8.

Collins, M., and Coauthors, 2010: The impact of global warming on the tropical Pacific Ocean and El Niño. *Nat. Geosci.*, **3**, 391–397, doi:10.1038/ngeo868.

Deser, C., A. S. Phillips, and M. A. Alexander, 2010: Twentieth century tropical sea surface temperature trends revisited. *Geophys. Res. Lett.*, **37**, L10701, doi:10.1029/2010GL043321.

England, M. H., and Coauthors, 2014: Recent intensification of wind-driven circulation in the Pacific and the ongoing warming hiatus. *Nat. Climate Change*, **4**, 222–227, doi:10.1038/nclimate2106.

Gates, W. L., and Coauthors, 1999: An overview of the results of the Atmospheric Model Intercomparison Project (AMIP I). *Bull. Amer. Meteor. Soc.*, **80**, 29–55, doi:10.1175/1520-0477(1999)080<0029:AOOTRO>2.0.CO;2.

Horel, J. D., and J. M. Wallace, 1981: Planetary-scale atmospheric phenomena associated with the Southern Oscillation. *Mon. Wea. Rev.*, **109**, 813–829, doi:10.1175/1520-0493(1981)109<0813:PSAPAW>2.0.CO;2.

Huang, P., and J. Ying, 2015: A multimodel ensemble pattern regression method to correct the tropical Pacific SST change patterns under global warming. *J. Climate*, **28**, 4706–4723, doi:10.1175/JCLI-D-14-00833.1.

——, S.-P. Xie, K. Hu, G. Huang, and R. Huang, 2013: Patterns of the seasonal response of tropical rainfall to global warming. *Nat. Geosci.*, **6**, 357–361, doi:10.1038/ngeo1792.

Johnson, N. C., and S.-P. Xie, 2010: Changes in the sea surface temperature threshold for tropical convection. *Nat. Geosci.*, **3**, 842–845, doi:10.1038/ngeo1008.

Kim, S. T., W. Cai, F.-F. Jin, A. Santoso, L. Wu, E. Guilyardi, and S.-I. An, 2014: Response of El Niño sea surface temperature variability to greenhouse warming. *Nat. Climate Change*, **4**, 786–790, doi:10.1038/nclimate2326.

Kosaka, Y., and S.-P. Xie, 2013: Recent global-warming hiatus tied to equatorial Pacific surface cooling. *Nature*, **501**, 403–407, doi:10.1038/nature12534.

L'Heureux, M. L., S. Lee, and B. Lyon, 2013: Recent multidecadal strengthening of the Walker circulation across the tropical Pacific. *Nat. Climate Change*, **3**, 571–576, doi:10.1038/nclimate1840.

Li, G., S.-P. Xie, Y. Du, and Y. Luo, 2016: Effects of excessive equatorial cold tongue bias on the projections of tropical Pacific climate change. Part I: The warming pattern in CMIP5 multi-model ensemble. *Climate Dyn.*, doi:10.1007/s00382-016-3043-5, in press.

Lin, Y., M. Zhao, and M. Zhang, 2015: Tropical cyclone rainfall area controlled by relative sea surface temperature. *Nat. Commun.*, **6**, 6591, doi:10.1038/ncomms7591.

Liu, Z., S. Vavrus, F. He, N. Wen, and Y. Zhong, 2005: Rethinking tropical ocean response to global warming: The enhanced equatorial warming. *J. Climate*, **18**, 4684–4700, doi:10.1175/JCLI3579.1.

Long, S.-M., S.-P. Xie, and W. Liu, 2016: Uncertainty in tropical rainfall projections: Atmospheric circulation effect and the ocean coupling. *J. Climate*, **29**, 2671–2687, doi:10.1175/JCLI-D-15-0601.1.

Ma, J., and S.-P. Xie, 2013: Regional patterns of sea surface temperature change: A source of uncertainty in future projections of precipitation and atmospheric circulation. *J. Climate*, **26**, 2482–2501, doi:10.1175/JCLI-D-12-00283.1.

McPhaden, M. J., S. E. Zebiak, and M. H. Glantz, 2006: ENSO as an integrating concept in Earth science. *Science*, **314**, 1740–1745, doi:10.1126/science.1132588.

Neale, R. B., and Coauthors, 2010: Description of the NCAR Community Atmosphere Model (CAM4). NCAR Tech. Note NCAR/TN-485+STR, 212 pp. [Available online at www.cesm.ucar.edu/models/ccsm4.0/cam/docs/description/cam4_desc.pdf.]

Ogata, T., S.-P. Xie, A. Wittenberg, and D.-Z. Sun, 2013: Interdecadal amplitude modulation of El Niño–Southern Oscillation and its impacts on tropical Pacific decadal variability. *J. Climate*, **26**, 7280–7297, doi:10.1175/JCLI-D-12-00415.1.

Philander, S. G., 1990: *El Niño, La Niña and the Southern Oscillation*. Academic Press, 293 pp.

Power, S., F. Delage, C. Chung, G. Kociuba, and K. Keay, 2013: Robust twenty-first-century projections of El Niño and related precipitation variability. *Nature*, **502**, 541–545, doi:10.1038/nature12580.

Rashid, H. A., A. C. Hirst, and S. J. Marsland, 2016: An atmospheric mechanism for ENSO amplitude changes under an abrupt quadrupling of CO_2 concentration in CMIP5 models. *Geophys. Res. Lett.*, **43**, 1687–1694, doi:10.1002/2015GL066768.

Stevenson, S. L., 2012: Significant changes to ENSO strength and impacts in the twenty-first century: Results from CMIP5. *Geophys. Res. Lett.*, **39**, L17703, doi:10.1029/2012GL052759.

Taylor, K. E., R. J. Stouffer, and G. A. Meehl, 2012: An overview of CMIP5 and the experiment design. *Bull. Amer. Meteor. Soc.*, **93**, 485–498, doi:10.1175/BAMS-D-11-00094.1.

Tokinaga, H., S.-P. Xie, A. Timmermann, S. McGregor, T. Ogata, H. Kubota, and Y. M. Okumura, 2012: Regional patterns of tropical Indo-Pacific climate change: Evidence of the Walker circulation weakening. *J. Climate*, **25**, 1689–1710, doi:10.1175/JCLI-D-11-00263.1.

Vecchi, G. A., and B. J. Soden, 2007a: Global warming and the weakening of the tropical circulation. *J. Climate*, **20**, 4316–4340, doi:10.1175/JCLI4258.1.

——, and ——, 2007b: Effect of remote sea surface temperature change on tropical cyclone potential intensity. *Nature*, **450**, 1066–1070, doi:10.1038/nature06423.

——, A. Clement, and B. J. Soden, 2008: Examining the tropical Pacific's response to global warming. *Eos, Trans. Amer. Geophys. Union*, **89**, 81–83, doi:10.1029/2008EO090002.

Watanabe, M., J.-S. Kug, F.-F. Jin, M. Collins, M. Ohba, and A. T. Wittenberg, 2012: Uncertainty in the ENSO amplitude change from the past to the future. *Geophys. Res. Lett.*, **39**, L20703, doi:10.1029/2012GL053305.

Wittenberg, A. T., 2009: Are historical records sufficient to constrain ENSO simulations? *Geophys. Res. Lett.*, **36**, L12702, doi:10.1029/2009GL038710.

——, A. Rosati, T. L. Delworth, G. A. Vecchi, and F. Zeng, 2014: ENSO modulation: Is it decadally predictable? *J. Climate*, **27**, 2667–2681, doi:10.1175/JCLI-D-13-00577.1.

Xie, S.-P., C. Deser, G. A. Vecchi, J. Ma, H. Teng, and A. T. Wittenberg, 2010: Global warming pattern formation: Sea surface temperature and rainfall. *J. Climate*, **23**, 966–986, doi:10.1175/2009JCLI3329.1.

——, and Coauthors, 2015: Towards predictive understanding of regional climate change. *Nat. Climate Change*, **5**, 921–930, doi:10.1038/nclimate2689.

Zhou, Z.-Q., S.-P. Xie, X.-T. Zheng, Q. Liu, and H. Wang, 2014: Global warming–induced changes in El Niño teleconnections over the North Pacific and North America. *J. Climate*, **27**, 9050–9064, doi:10.1175/JCLI-D-14-00254.1.